Springer

KSME

Journal of Mechanical Science and Technology 31 (11) (2017) 5291~5298
www.springerlink.com/content/1738-494x(Print)/1976-3824(Online)
DOI 10.1007/s12206-017-1023-2

Computational study of radial gap effect between impeller and diffuser on the unsteadiness of vaned diffuser in a centrifugal compressor †

Anish S.[1,*] and N. Sitaram[2]

[1]*Turbomachines Laboratory, Department of Mechanical Engineering, National Institute of Technology Karnataka, Mangalore, 575025, India*
[2]*Turbomachines Laboratory, Department of Mechanical Engineering, IIT Madras, Chennai-600036, India*
(Present Address: School of Aeronautical Sciences, Hindustan Institute of Technology and Science, 1, Rajiv Gandhi Salai (OMR), Padur, (Via) Kelambakkam, Chennai-603103, India)

(Manuscript Received January 15, 2017; Revised June 1, 2017; Accepted July 28, 2017)

Abstract

Understanding the unsteady fluid dynamics inside the diffuser holds the key to improve the performance of centrifugal compressor. A detailed computational study has been conducted in a low-speed centrifugal compressor to understand the unsteady flow mechanisms that govern the static pressure recovery inside the vaned diffusers. Simulations are carried out for three different leading edge locations at design and off-design conditions. The study is carried out using Reynolds-averaged Navier-Stokes simulations. This study revealed that the unsteady fluctuations exhibit contrasting behavior at different radial gaps and flow coefficients. An optimum radial gap is strictly a function of the stage loading. A high radial gap helps contain the fluctuations at low flow coefficients, but it enhances the fluctuations at high flow coefficients. If the leading edge is kept close to the impeller blade, then the above design flow coefficient of the vaned passage facilitates a reduction in the unsteady fluctuations. On the contrary, keeping the leading edge close to the impeller blade can accelerate the unsteady fluctuations at low flow coefficients.

Keywords: Centrifugal compressor; Vaned diffuser; Leading edge location; Computational investigations; Unsteady flow

1. Introduction

A more efficient compressor requires an accurate and detailed understanding of the coupled flow behavior and incorporates the same in the design stage itself. Current centrifugal compressors are designed for steady relative flows; however, the flow is unsteady in reality. Steady state implies that the simulations are carried out at a particular instant of time. Steady-state simulations neglect the effects of spatial unsteadiness due to the relative position of the impeller blade and diffuser vane, as well as the temporal unsteadiness caused by turbulence. This study attempts to understand the influence of unsteady impeller wake on the diffuser flow.

The non-uniform flow at the impeller outlet is unsteady to the stationary diffuser. The diffuser imposes an unsteady backpressure on the rotating impeller. In addition to the periodic disturbances with the rotational or blade passing frequency, instabilities can develop in the centrifugal compression systems in the form of rotating stall and surge. Several researchers have investigated the importance of this unsteadiness [1-10]. Krain [4] observed that the unsteadiness was at maximum ahead of the diffuser blades and less in the Vaned diffuser (VD) area aft of the diffuser throat. This phenomenon was in contrast to the observations made by Justen et al. [1], where maximum unsteadiness was found in the vaned region. They also observed that in the downstream of the diffuser channel, the unsteadiness was not diminishing and pressure fluctuations were distinctly higher than that in the vaneless space. The magnitude of unsteady fluctuations depends on the operating point. The aperiodic unsteadiness rapidly decreases downstream of the diffuser channel. Moreover, the aperiodic unsteadiness becomes relatively significant, particularly at off-design conditions due to the large incidence angle at the diffuser vane leading edge [5]. Bulot and Trébinjac [6] showed that the unsteadiness was due to the jet and wake flow structure emerging from the radial impeller, as well as the pressure waves from the interaction between the vane bow shock wave and the impeller blade. Zamiri et al. [7] captured the pressure fluctuation spectra at the impeller-diffuser interface to analyze the noise characteristics of the centrifugal compressor. Benichou et al. [8] exposed the limitations in accurately predicting the separated flows inside a VD.

The radial gap between the impeller and diffuser is an important parameter in centrifugal compressor design. The radial

*Corresponding author. Tel.: +91 9036317552, Fax.: +91 824 2474033
E-mail address: anish@nitk.edu.in
† Recommended by Associate Editor Donghyun You

Table 1. Design details of the centrifugal compressor.

Pressure rise, Δp	350 mm WC
Speed, N	3000 rpm
Inducer hub diameter, d_{1h}	110 mm
Blade angle at inducer hub, β_{1h}	45°
Impeller outlet diameter, d_2	393 mm
Number of impeller blades, Z	20
Diffuser LE diameter, d_3 for $R_3 = 1.05$	412.65 mm
Diffuser LE diameter, d_3 for $R_3 = 1.10$	432.3 mm
Diffuser LE diameter, d_3 for $R_3 = 1.15$	451.95
Diffuser outlet diameter, d_5	600 mm
Mass flow, m	0.53 kg/s
Shape number, N_{sh}	0.084
Inducer tip diameter, d_{1t}	225 mm
Blade angle at inducer tip, β_{1t}	29°
Impeller blade outlet angle, β_2	90°
Number of diffuser vanes, Z_d	22
Diffuser TE diameter, d_4 for $R_3 = 1.05$	472.15 mm
Diffuser TE diameter, d_4 for $R_3 = 1.10$	491.8 mm
Diffuser TE diameter, d_4 for $R_3 = 1.15$	511.45 mm
Width of diffuser passage, b_2	20 mm

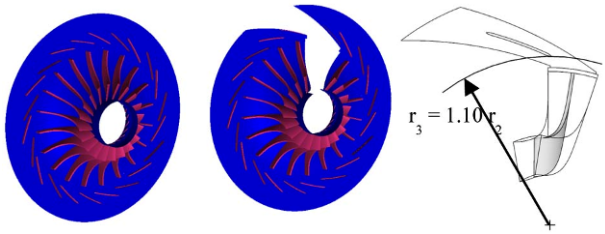

(a) (b) (c)

Fig. 1. (a) 3D view of the impeller blades and diffuser vane fitted on the hub wall; (b) with the removal of one set of impeller blade and diffuser vane; (c) one set of impeller and diffuser vane passage showing the leading edge location of the diffuser vane.

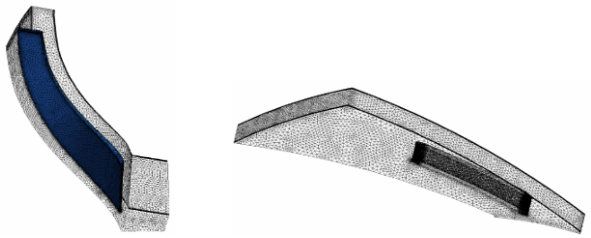

(a) Impeller passage (b) Diffuser passage

Fig. 2. Mesh generated with unstructured tetrahedral elements used for meshing.

gap can be varied by keeping the diffuser vane leading edge at different radial locations (R_3). As the radial gap increases, the flow path becomes long, thereby increasing the boundary layer thickness at the throat region. This effect causes increased blockage in the diffuser throat. Apart from this effect, radial gap variation affects the diffuser throat area and size of the machine, consequently affecting the compressor pressure ratio, efficiency, and mass flow range. Ziegler et al. [11] found that the choke mass flow rate decreases with reduced R_3 and increases the total pressure ratio with decreasing radial gap. A small radial gap may lead to a more homogeneous flow field at the diffuser vane exit and a high diffuser pressure recovery, resulting in high compressor efficiency. Many researchers have presented investigations on radial gap variations [12-15], but corresponding recommendations to find an optimum radial gap at design and off-design points based on the unsteady nature of the flow do not exist yet. The objective of this work is to computationally analyze the unsteady behavior of the flow through a conventional VD. The leading edge of the diffuser is kept at three different locations, and the simulations are carried out at the design and off-design conditions.

2. Details of the centrifugal compressor

A low-speed centrifugal compressor with a VD is selected for the present study. The compressor has a radial impeller with 20 blades. The impeller outer diameter is 393 mm, whereas the diffuser outlet diameter is 600 mm. The diffuser passage has a constant width of 20 mm with a rectangular cross section. Vanes are fixed on the hub wall. Table 1 provides more specifications of the compressor.

Fig. 1 shows the 3D view of the low-speed compressor with VDs. The diffuser has 22 vanes and 20 impeller blades. The chord to spacing ratio is 1.4 for the diffuser vanes.

The angles are measured with reference to the tangential direction. The leading edge shape is made semi-elliptical with major axis four times the minor axis. The minor axis is the thickness of the vane and is equal to 4 mm. The trailing edge is also a semi-elliptical shape with a major axis of 16 mm and a minor axis of 4 mm. The leading edge of the diffuser vane is kept at three different radial locations, namely $R_3 = r_3/r_2 = 1.05$, 1.10 and 1.15. A vaneless portion is found after the trailing edge of the diffuser vane. The outer radius of this vaneless portion is fixed and is common for all the configurations. The diffuser vane angle is set in such a way that the incidence angle is zero at the design flow coefficient at each location. Impeller tip clearance is set as 2 % of the impeller width at the outlet.

3. Computational methodology

The numerical simulation of the entire impeller blades and diffuser passage requires a considerable amount of computational time and computer memory. Thus, the physical model used for the computational simulation consists of a single diffuser vane and a single impeller blade passage to avoid this problem. Unstructured tetrahedral elements are used for meshing. Fine elements are provided around the impeller blade, diffuser vanes, and near the hub and shroud walls. Very fine elements are provided at the leading edge, trailing edge, and at

the tip clearance region (Fig. 2). Prism layers are attached to the walls. At least six prism layers are kept in the tip clearance region. Geometry modeling and meshing are conducted using ICEM CFD. The Octree method is used to generate tetra mesh using a top-down meshing approach.

The meshes for the impeller and diffuser are separately created and imported into the CFX-Pre as two separate components. A diffuser is defined as a stationary component, whereas an impeller is defined as a rotating component with 3000 rpm. The working fluid used for the simulation is air, which is treated as an ideal gas. Air is compressible, thereby allowing the usage of state equation as one more governing equation to solve density. The reference pressure is set as 101.325 kPa, which is equal to the local atmospheric pressure. All relative pressure specifications set in ANSYS CFX are measured relative to this reference pressure value. When boundary and initial conditions are specified, they are set relative to the reference pressure.

Menter [16] suggested the use of advanced ω-based models, such as the Spalart-Allmaras or the SST model, to obtain more realistic results for flows with adverse pressure gradients and pressure-induced separation. Accordingly, the SST-$k\omega$ turbulence model is used with y+ values less than 2 at the walls for the present simulations. This simulation has been achieved by putting very fine prism layers close to the wall. In the present case, the compressor takes air from the atmosphere. Hence, the inlet conditions are known. Uniform total pressure and temperature have been provided as inlet boundary conditions. Specification of uniform inflow normal to the inlet plane is relatively justified because the inlet boundary is sufficiently moved away upstream of the impeller. This method has been adopted from Smirnov et al. [13]. At the outlet, the mass flow rate is specified. Each simulation is performed at a constant mass flow rate. Other boundaries, namely hub, shroud, impeller blade, and diffuser vane, are specified as adiabatic wall type boundaries. The impeller shroud wall is stationary; hence, its wall influence on flow is considered to be a counter-rotating mode. Therefore, in a stationary frame of reference, the shroud is stationary. Apart from impeller shroud, all other walls are specified with no slip condition.

The transient relative motion between the impeller and diffuser on each side of the interface is simulated. ANSYS CFX uses a coupled solver, which solves the hydrodynamic equations as a single system. This solver uses a fully implicit discretization of the governing equations at any given time step. The governing equations are the transport equations of mass, momentum, energy, turbulence kinetic energy, and turbulence eddy frequency. Time period "T" is defined as the required time for an impeller blade to cover one diffuser passage. This time period is divided into 22 time steps for an impeller speed of 3000 rpm. The time period $T = 0.000909$ s and time step for each case is given as $\Delta t = 4.13 \times 10^{-5}$ s. The transient simulations are performed for 1000 time steps, which means that the time duration is 4.13×10^{-2}. At each time step, a result file is obtained.

Table 2. Grid independence study for impeller.

	No. of elements	P_2/P_{01}	P_{02}/P_{01}	P_2/P_{01} % difference	P_{02}/P_{01} % difference
Grid 1	999402	1.0182	1.039	-	-
Grid 2	657118	1.0182	1.039	0.003 %	0.010 %
Grid 3	351682	1.0178	1.038	0.042 %	0.077 %

Table 3. Grid independence study for VD.

		No. of elements	c_p	% difference
VD $R_3 = 1.05$	Grid 1	652142	0.6372	-
	Grid 2	421003	0.6371	0.03 %
	Grid 3	285148	0.6285	1.37 %
VD $R_3 = 1.10$	Grid 1	635874	0.6217	-
	Grid 2	481719	0.6213	0.06 %
	Grid 3	298556	0.6151	1.06 %
VD $R_3 = 1.15$	Grid 1	634578	0.5825	-
	Grid 2	445862	0.5822	0.05 %
	Grid 3	289523	0.5748	1.32 %

4. Grid independence study

Detailed grid independency studies are separately carried out for the impeller and diffuser. Three different types of grids are used. These grids are at three different levels: Grid 1 for fine, grid 2 for medium, and grid 3 for coarse mesh. Table 2 shows the grid-independent study for the impeller. Herein, pressure ratios P_2/P_{01} and P_{02}/P_{01} are compared for the three different grids. Grid 1 is taken as the reference, and the pressure ratio obtained with this grid is compared to that of the two other grids. Table 2 shows the percentage differences. The differences are considerably less for grid 2 when compared with grid 3.

In the case of the diffuser, the pressure recovery coefficient (c_p) is taken as the parameter for comparison between different grids. The VD has three configurations ($R_3 = 1.05$, 1.10 and 1.15). Hence, the grid independence study has to be separately conducted for each configuration. In all these cases, three different sets of grids have been selected. Table 3 shows the comparison of the c_p values. For $R_3 = 1.05$, the c_p value of grid 2 has 0.031 % difference compared with grid 1. For $R_3 = 1.10$, the difference between grids 2 and 1 is 0.06 %, and for $R_3 = 1.15$, the difference is 0.052 %. Grid 3 is a coarse mesh in all these cases, and its c_p value is slightly higher compared with that of grid 1. From these analyses, grid 2 has been selected for further numerical simulations.

5. Validations

The present study adopted the validation methodology similar to Smirnov et al. [13], Boncinelli et al. [14] and Guo et al. [15]. They have compared the time-averaged and the steady-state values with the experimental results. The steady-state

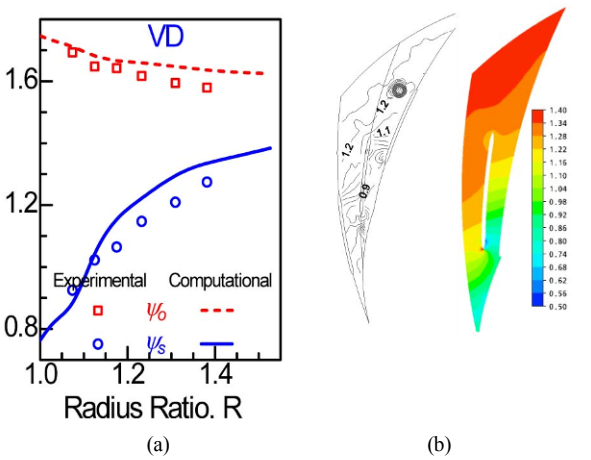

Fig. 3. (a) Radial variation of $\overline{\overline{\psi}}_s$ and $\overline{\overline{\psi}}_o$ at design flow coefficient (ϕ = 0.34); (b) static pressure coefficient contours at the diffuser hub wall. The color plot represents CFD, whereas the black and white plot represents experiment.

simulations are conducted using a frozen rotor approach. The results obtained from the steady-state simulations are then provided as an initial value file to the unsteady simulation. The separated flow region mainly appears at off-design operating conditions. Hence, the validation has been conducted at design as well as off-design conditions. For the present study, the computational results are compared with the results obtained by Issac et al. [16]. Fig. 3(a) shows the variation of mass-averaged total ($\overline{\overline{\psi}}_o$) and static pressure ($\overline{\overline{\psi}}_s$) coefficient with respect to radius ratio, R, across the diffuser. Good agreement is obtained between computational and experimental values. In addition, the computational results with the experimental values are compared with the static pressure coefficient at the hub wall of the diffuser (Fig. 3(b)). The stagnation zones and the radial pressure gradient are predicted with good accuracy in the present simulations.

6. Results and discussions

6.1 Overall stage performance

The total to static pressure ratio is plotted at different time steps for all the diffuser configurations to understand the unsteady effects in the overall stage performance. Fig. 4 compares the total to static pressure ratio across the stage at different time steps at three different R_3 values, which are instantaneous values of stage pressure rise. The time required for the impeller to pass one diffuser vane is divided into 22 time steps. The pressure rise is small because the compressor used for the study is a low-speed compressor, and the absolute values of pressure are taken to calculate the ratio. The unsteady variations are small at ϕ = 0.23 for a diffuser leading edge location of R_3 = 1.15. The unsteady fluctuations become large below the design flow coefficient because the radial gap decreases. The deviations from the mean value are minimum at R_3 = 1.10 at the design flow coefficient. For R_3 = 1.05, the unsteadiness

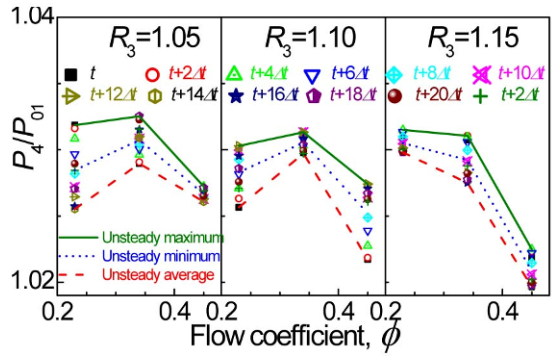

Fig. 4. Total to static pressure ratio at different time steps.

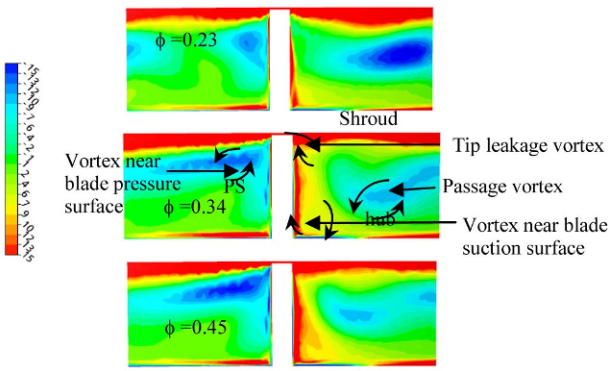

Fig. 5. Normalized streamwise vorticity contours just before impeller blade trailing edge (M = 0.96); PS = Pressure surface, SS = Suction surface.

is small at ϕ = 0.45. These observations indicate that the unsteady variations are minimal at certain optimum R_3 values for a particular flow coefficient.

6.2 Interaction of impeller vortices with the diffuser vane

At the impeller exit, the flow is highly non-uniform due to passage, tip leakage, and trailing edge vortices from the impeller blade. These vortices are convected into the diffuser passage and interact with diffuser vanes. The resultant of these vortices along the streamwise direction (flow direction) is calculated and normalized with respect to the impeller outlet diameter and the design tip speed. Fig. 5 shows the normalized streamwise vorticity contour at the outlet of the impeller blade. The normalization is made with respect to the impeller outlet diameter and the rotor tip speed at design conditions. The streamwise vorticity may be either positive or negative depending on the direction of the rotation. The right-hand thumb rule provides the direction of rotation. A positive streamwise vorticity refers to a counterclockwise rotation, where the rotation axis lies along the flow direction. Similarly, negative streamwise vorticity refers to clockwise rotation.

At ϕ = 0.23, the incidence at the diffuser vane leading edge is treated as positive, and the stagnation point slightly moves toward the upper convex portion of the diffuser vane. The

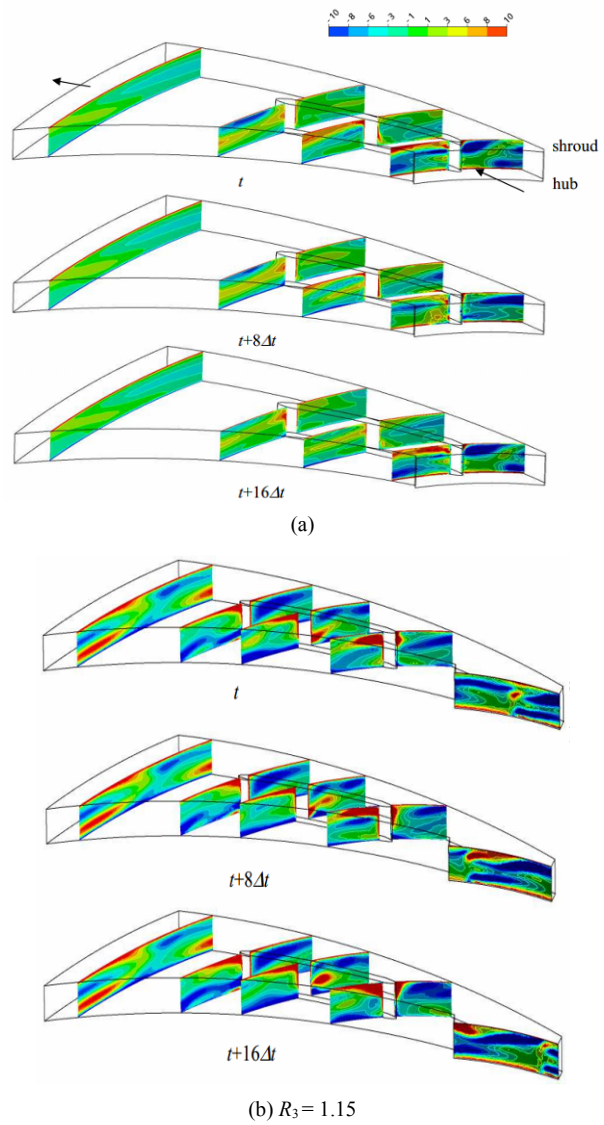

Fig. 6. Normalized streamwise vorticity contours for VD at below design point (ϕ = 0.23) for (a) R_3 = 1.05; (b) R_3 = 1.15.

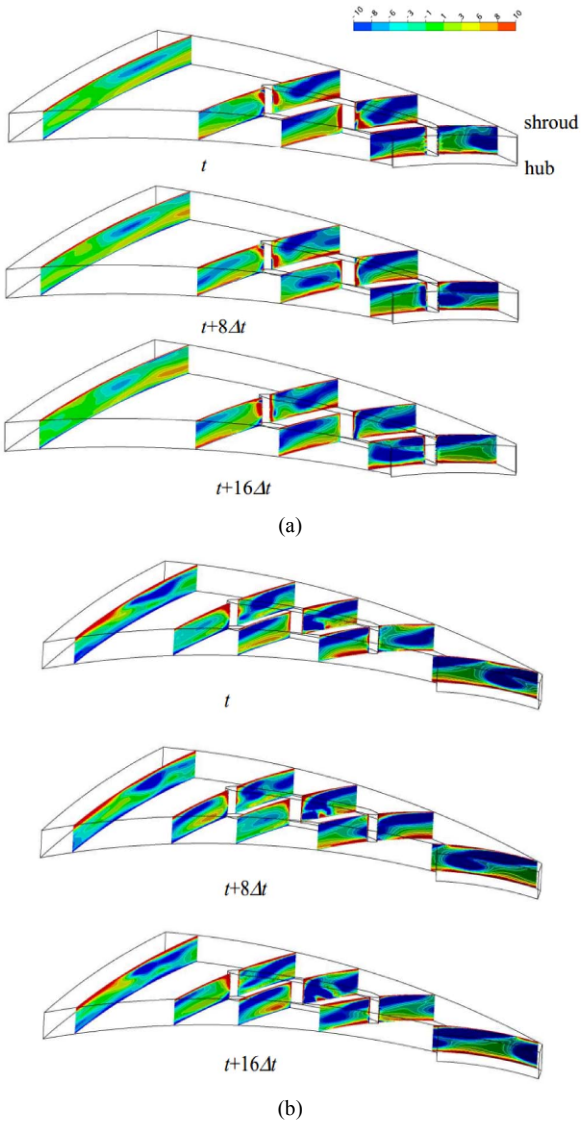

Fig. 7. Normalized streamwise vorticity contours for VD at the above design point (ϕ = 0.45) for (a) R_3 = 1.05; (b) R_3 = 1.15.

flow takes a turn around the small radius at the diffuser vane leading edge, resulting in vortex formation from the leading edge. These leading edge vortices are mainly observed near the shroud wall of the diffuser passage (Fig. 6).

From the impeller exit, the vortices with different sense of rotations (positive and the negative) approach the diffuser vane leading edge one after another at frequent intervals and interact with the leading edge vortices of the diffuser vane. The vortex at the diffuser vane leading edge, which is created by a positive incidence, rotates in a counterclockwise direction. Hence, a positive vortex from the impeller enhances the diffuser vane leading edge vortex, whereas the negative vortex weakens the leading edge vortex (Fig. 6(a)). At $t + 8\Delta t$, the corner of the shroud pressure surface side shows a weak positive vortex region. The core of the leading edge vortex moves from the corner of the shroud suction side to the hub pressure surface side. This movement is under the influence of the strong negative vortex region from the impeller. The vortices lose their unsteady nature inside the vaned passage due to circumferential mixing.

At R_3 = 1.15, the large vaneless region between the impeller blade and diffuser vane allows mixing of the positive and negative vortices before they reach the diffuser vane leading edge. The tip leakage and blade trailing edge vortices have a different rotation than the passage vortex, and the relative strength varies with the flow coefficient. The leading edge vortex at the diffuser vane is positive in the streamwise direction and becomes weakened by its interaction with the mean stream flow, whose streamwise vorticity component is mostly negative (Fig. 6(b)). The separated flow region does not extend throughout the chord length of the vane and does not spread to the shroud as observed with R_3 = 1.05. Fig. 6(b)

shows that the strength of the vorticity contours varies at the diffuser inlet region but not within the passage. This phenomenon indicates that the unsteady nature of the vortex flow reduces in the vaned passage. The large radial gap between the impeller blade and diffuser vane helps to reduce the unsteadiness in the vaned passage.

At the above design point, the incidence is negative, especially near the hub, and the stagnation point slightly moves toward the lower concave side of the diffuser vane. The leading edge vortex formed at the hub-pressure side corner is negative (Fig. 7(a)), and the endwall vortices have a strong positive streamwise component near the hub. The interaction of the endwall vortices weakens the leading edge vortices.

In $R_3 = 1.15$ configuration, the incidence angle near the hub is relatively higher than $R_3 = 1.05$. The flow moves around the leading edge, thus creating a sudden acceleration zone. The adverse pressure gradient created through this depression causes strong vortex from the vane pressure surface. The strength of this negative leading edge vortex is high and separates from the vane pressure surface while interacting with the upstream impeller flow (Fig. 7(b)). The positive vortex region from the impeller side interacts with the vortex from the vane pressure surface, which can be observed from the streamwise vorticity contours. As a result of this interaction, a small positive vortex region is formed near the hub, which reduces the strength of the negative vorticity near the vane pressure surface.

6.3 Unsteady pressure fluctuations in vaned diffuser

The unsteady fluctuations in the diffuser can be attributed to the interaction with the rotating impeller. The level of unsteadiness is quantified by taking the Root mean square (RMS) value of the fluctuating component of pressure (p') along the diffuser passage. The RMS value of pressure fluctuation (p'_{RMS}) at different time steps has been calculated and plotted along with the fluctuations for various configurations.

Fig. 8 shows the fluctuating component of pressure (p') for all configurations at different flow coefficients. Variations of p'_{RMS} value suggest a high level of unsteadiness flow in the vaneless space region. Once the flow reaches the leading edge and enters into the geometric throat, the fluctuations decrease. At the exit of the diffuser, a periodic part of the fluctuation is present, but the aperiodic part is liable to diminish in the vaned portion of the diffuser passage. If separations from the diffuser vane exist, then the aperiodic fluctuations increase in the diffuser channel. For $R_3 = 1.05$, p'_{RMS} is lower for $\phi = 0.45$ at the exit of the diffuser compared with other flow coefficients. At strong interaction (R_3=1.05), $\phi = 0.45$ shows a better performance. The improved performance of the VD at this flow coefficient can be related to the low value of fluctuations. At $\phi = 0.23$, large fluctuations are observed in the interaction region. At R = 1.175, the fluctuations decrease before they increase again. Some periodicities in the fluctuations are observed at the inlet of the diffuser domain. Time steps t and $t + 22\Delta t$ stand for the same relative positions of the impeller and diffuser. If the fluctuations are caused by the rotation of the impeller alone, then the fluctuations will also be purely periodic. The extent of deviation from the periodicity depends on the level of aperiodic disturbances in the flow. At the exit of the diffuser, trailing edge vortices and vortices from the separated flow region add to increased disturbances to the flow.

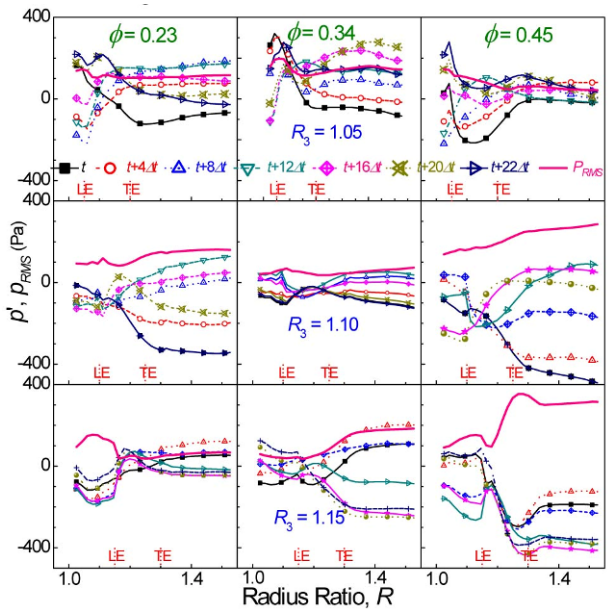

Fig. 8. Radial variation of unsteady pressure fluctuations and RMS value of the fluctuations for VD.

At $R_3 = 1.10$, the pressure fluctuations are high at the exit of the diffuser at off-design conditions. At $\phi = 0.23$ and $\phi = 0.45$, the RMS value at the diffuser exit is slightly higher than that at the inlet. At the leading edge, the fluctuations decrease and then increase again. Unsteadiness is considerably large at the exit of the diffuser at $\phi = 0.45$ due to flow separation from the diffuser vane. The design flow coefficient ($\phi = 0.34$) shows least pressure fluctuations; hence, the static pressure rise is relatively high in this configuration due to reduced losses. The p'_{RMS} is nearly constant in the VD passage in this case.

For $R_3 = 1.15$, the fluctuations are reduced in the vaned passage. However, before the leading edge and after the trailing edge, large values of fluctuations are observed. At $\phi = 0.23$, p'_{RMS} is high before the leading edge. However, once the flow enters the vaned passage, fluctuations are suppressed due to the flow guidance provided by the vanes. At $\phi = 0.34$, though less fluctuations are observed in the vaneless space toward the exit, p'_{RMS} increases. Maximum p'_{RMS} is observed at $\phi = 0.45$. A sudden rise in p'_{RMS} occurred due to the separated flow, particularly after the leading edge.

These variations suggest that an optimum diffuser vane leading edge location (radial gap between the impeller and diffuser) is strictly a function of the flow coefficient. In the above and below design flow coefficients, the diffuser exhibits contrasting unsteady behavior with the three selected diffuser

configurations.

7. Conclusions

A computational study has been undertaken to understand the unsteady flow behavior inside a VD under different operating conditions. The diffuser vane is kept at three different radial locations, and an optimum location is basically a function of the flow coefficient.

At the above design flow coefficient, if the leading edge is kept at R_3=1.05, then the vaned passage facilitates a reduction in the unsteady fluctuations. Consequently, the p'_{RMS} value decreases toward the diffuser exit. On the contrary, keeping the leading edge close to the impeller blade can accelerate the unsteadiness at low flow coefficients. Similarly, an increase in the radial gap helps to contain the fluctuations at low flow coefficients, but enhances the fluctuations at high flow coefficients. These contrasting behaviors are attributed to the interactions of the upstream, unsteady streamwise vortices from the impeller passage with the diffuser vane.

No single value of optimum radial gap for a compressor is present, but it relies on the flow coefficient of the machine. The present conclusions are based on studies on a low-speed centrifugal compressor with circular arc diffuser vane. Therefore, further studies have to be conducted on a high-specific speed compressor.

Nomenclature

M : Normalized streamwise distance
p : Pressure (Pa)
p' : Fluctuating pressure (Pa)
p'_{RMS} : RMS value of p' (Pa)
R : Radius ratio
r : Radius (mm)
S : Normalized span-wise distance
ϕ : Flow coefficient = C_{m2}/U_2
$\overline{\overline{\psi}}_o$: Mass averaged pressure coefficient

Subscript

0 : Total state
1 : Inlet
2 : Impeller TE
3 : Diffuser vane LE
4 : Diffuser outlet
s : Static state

References

[1] F. Justen, K. U. Ziegler and H. E. Gallus, Experimental investigation of unsteady flow phenomena in a centrifugal compressor vaned diffuser of variable geometry, *ASME Journal of Turbomachinery*, 121 (1999) 763-771.

[2] V. Filipenco, S. Deniz, J. Johnston, E. Greitzer and N. Cumpsty, Effects of inlet flow field conditions on the performance of centrifugal compressor diffusers: Part 1 - Discrete-passage diffuser, *ASME Journal of Turbomachinery*, 122 (2000) 1-10.

[3] S. Deniz, E. M. Greitzer and N. A. Cumpsty, Effects of inlet flow field conditions on the performance of centrifugal compressor diffusers: Part 2 - Straight channel diffuser, *ASME Journal of Turbomachinery*, 122 (2000) 11-21.

[4] H. Krain, Unsteady diffuser flow in a transonic centrifugal compressor, *International Journal of Rotating Machinery*, 8 (3) (2002) 223-231.

[5] J. S. Kang and S. H. Kang, Steady and unsteady flow phenomena in a channel diffuser of a centrifugal compressor, *JSME International Journal, Series B*, 47 (2004) 91-100.

[6] N. Bulot and I. Trébinjac, Effect of the unsteadiness on the diffuser flow in a transonic centrifugal compressor stage, *International Journal of Rotating Machinery*, 2009 (2009).

[7] A. Zamiri, B. J. Lee and J. T. Chung, Numerical evaluation of the unsteady flow in a centrifugal compressor with Vaned diffuser via URANS approach. GT2016-57538, *ASME Turbo Expo 2016: Turbomachinery Technical Conference and Exposition*, Seoul, South Korea, June 13-17 (2016).

[8] E. Benichou and I. Trébinjac, Comparison of steady and unsteady flows in a transonic radial vaned diffuser, *ASME Journal of Turbomachinery*, 138 (12) (2016) Article ID 121002.

[9] Y. Bousquet, X. Carbonneau, G. Dufour, N. Binder and I. Trebinjac, Analysis of the unsteady flow field in a centrifugal compressor from peak efficiency to near stall with full-annulus simulations, *International Journal of Rotating Machinery*, 2014 (2014) Article ID 729629.

[10] S. Ibaraki, T. Matsuo and T. Yokoyama, Investigation of unsteady flow field in a vaned diffuser of a transonic centrifugal compressor, *ASME Journal of Turbomachinery*, 129 (2007) 686-693.

[11] K. U. Ziegler, H. E. Gallus and R. Niehuis, A study on impeller diffuser interaction-Part II: Detailed flow analysis, *ASME Journal of Turbomachinery*, 125 (2003) 183-192.

[12] M. Inoue and N. A. Cumpsty, Experimental study of centrifugal impeller discharge flow in vaneless and vaned diffusers, *ASME Journal of Engineering Gas Turbines Power*, 106 (1984) 455-467.

[13] D. Jin, Z. Jiang, H. Hasemann, U. Haupt and M. Rautenberg, Influence of vaned diffuser on dangerous blade vibration due to blade flow interactions in a centrifugal compressor, *ASME Paper 95-GT-122* (1995).

[14] Y. K. P. Shum, C. S. Tan and N. A. Cumpsty, Impeller-diffuser interaction in centrifugal compressor, *ASME Journal of Turbomachinery*, 122 (2000) 777-786.

[15] J. W. Salvage, Development of centrifugal compressor with a variable geometry split-ring pipe diffuser, *ASME Journal of Turbomachinery*, 121 (1999) 295-303.

[16] F. R. Menter, Two-equation eddy-viscosity turbulence models for engineering applications, *AIAA-Journal*, 32 (1994) 1598-1605.

[17] V. D. Villanueva and V. D. Alfonso, Characterization of the flow field response to vaneless space reduction in centrifugal compressors, *M.S. Thesis,* Department of Aeronautics and Astronautics, Massachusetts Institute of Technology (2006).

[18] P. E. Smirnov, T. Hansen and F. R. Menter, Numerical simulation of turbulent flows in centrifugal compressor stages with different radial gaps, *ASME GT2007-27376* (2007).

[19] P. Boncinelli, M. Ermini, S. Bartolacci and A. Arnone, Impeller-diffuser interaction in centrifugal compressors: numerical analysis of Radiver test case, *Journal of Propulsion and Power*, 23 (2007) 1304-1312.

[20] Q. Guo, H. Chen, X.-C. Zhu, Z.-H. Du and Y. Zhao, Numerical simulations of a stall inside a centrifugal compressor, *Proc. Instn. Mech. Engrs, Part A: Journal of Power and Energy*, 221 (2007) 683-693.

[21] J. M. Issac, N. Sitaram and M. Govardhan, Effect of diffuser vane height and position on the performance of a centrifugal compressor, *Proc. Instn. Mech. Engrs, Part A: J. Power and Energy*, 218 (2004) 647-654.

S. Anish received his Ph.D. from the Indian Institute of Technology Madras (IIT Madras). He is currently an Assistant Professor at the National Institute of Technology Karnataka, India. His research interests are fluid dynamics, thermodynamics, and turbomachinery aerodynamics.